ChemPubSoc Europe

DOI: 10.1002/cphc.201600789

CHEMPHYSCHEM Articles

Growth Kinetics in Layer-by-Layer Assemblies of Organic Nanoparticles and Polyelectrolytes

Maziar Mohammadi,[a] Ali Salehi,[b] Ryan J. Branch,[b] Lucas J. Cygan,[b] Cagri G. Besirli,[c] and Ronald G. Larson*[a, b]

The growth rates of layer-by-layer (LbL) assemblies of polyelectrolytes (PEs) with oppositely charged polystyrene (PS) nanoparticles (NPs) as a function of molecular weight (MW) of the PEs, ionic strength of the media, and NP size and charge are systematically investigated. To optimize LbL growth, the effects of suspension concentration, pH of the media, and deposition time on the growth rate of multilayers are assessed. Both linear and exponential growth behaviors are observed and, under optimal conditions, films of up to around 1 μm thick can readily be assembled after 10 or so bilayers have been deposited. For many of the cases studied, an intermediate MW of PE leads to the fastest film buildup, for both cationic poly(ethyleneimine) deposited alternately with anionic PS NPs and for anionic poly(acrylic acid) deposited alternately with cationic PS NPs. The existence of an optimal MW suggests that growth rate is determined by a balance of thermodynamic factors, including density of polymer bridges between particles, and kinetic factors, specifically the diffusivity of polymer in the film. The optimal MW, however, is very sensitive to the materials used. Moreover, depending on the MW of the PE, increasing salinity could increase or decrease the growth kinetics. Finally, the surface morphology of the films is characterized with AFM and SEM to reveal that the roughness increases less than linearly with film thickness.

1. Introduction

Functional thin films have attracted significant attention recently,[1,2] due to their versatility and ease of fabrication. One of the most flexible methods of assembling these films is by layer-by-layer (LbL) deposition, which is the alternating deposition of oppositely charged polyelectrolytes (PEs) or oppositely charged PEs and nanoparticles (NPs). LBL assembled thin films are easy to fabricate, inexpensive, and their properties can be finely tuned.[3,4] Furthermore, the process of making these films does not need to be performed under extreme conditions.[5]

Although the major driving force for LbL assembly is usually electrostatic interactions, other interactions, including hydrogen bonding, hydrophobic interactions, host–guest interactions, and covalent bonding, lead to the formation of such assemblies.[4,6] In electrostatically driven PE/PE assembly, LbL growth occurs due to charge overcompensation, that is, each film ingredient deposited on the surface reverses the surface charge, making it ready to adsorb the next LbL layer.[4] LbL assembly of PEs and organic NPs has considerable applications in drug delivery, coating, creation of three-dimensional scaffolds, and sensors, to name but a few.[4,7–16] However, little is known about the mechanism of their growth and its effective parameters. Thus, it is important to study PE/organic NP LbL films to better understand the effects of different parameters on their assembly and growth.

A major parameter that affects the growth kinetics of LbL films is the molecular weight (MW) of the PE. MW affects the diffusion of PE chains within the PE matrix and their mobility in the bulk solution. Moreover, MW influences the thermodynamic driving force for the diffusion and overall integrity of the LbL film. For PE/PE films, several studies have shown the dramatic effect of MW on the thickness and morphology.[17–20] Nestler et al. studied the effect of MW on the growth kinetics of poly(styrenesulfonate) (PSS)/poly(diallyldimethylammonium chloride) (PDADMAC) multilayer films.[17] Below a certain MW, they demonstrated that an increase in the MW of the polyanion (PSS) decreased both the film thickness and layer number at which the growth rate changed to the linear regime. However, they reported the completely opposite trend in response to a variation of the MW of the polycation (PDADMAC). Shen et al. studied the effect of the polyanion (hyaluronan) MW on the growth kinetics of poly(L-lysine)/hyaluronan LbL films.[18] In contrast to the results reported by Nestler et al.,[17] they showed that increasing the polyanion MW increased the film thickness. This reveals the complex effect of MW of the PE on

[a] M. Mohammadi, Prof. R. G. Larson
Department of Mechanical Engineering
University of Michigan
Ann Arbor, MI 48109 (USA)
E-mail: rlarson@umich.edu

[b] A. Salehi, R. J. Branch, L. J. Cygan, Prof. R. G. Larson
Department of Chemical Engineering
University of Michigan
Ann Arbor, MI 48109 (USA)

[c] Dr. C. G. Besirli
Department of Ophthalmology and Visual Sciences
Kellogg Eye Center, University of Michigan
Ann Arbor, MI 48105 (USA)

Supporting Information and the ORCID identification number(s) for the author(s) of this article can be found under http://dx.doi.org/10.1002/cphc.201600789.

LbL growth and suggests that it depends on the specific system being studied.

In contrast to PE/PE films, very few studies have addressed the effect of MW of the PE on the growth kinetics and surface morphology of PE/NP films and, even for these, the MW was not the main focus. Rahman and Taghavinia used poly(ethyleneimine) (PEI) with two different MWs (1.3 and 750 kg mol^{-1}) to grow PEI/TiO_2 NP composites.[3] They measured LbL growth by UV/Vis spectrophotometry and concluded that film growth was 25% slower when PEI with lower MW was employed. In another study by the same group, Rahman et al. showed greater deposition for PEI/TiO_2 NP composites with lower MW PEI.[21] They explained this opposite growth behavior by noting that the substrate and its geometry had important effects on film growth. In the later study, they grew composites on cellulose fibers, as opposed to the planar quartz sheets that they employed for the earlier work. They claimed that PEI with lower MW could diffuse into the porous structure of cellulose faster. In addition, they showed that films with lower MW of PEI had a less porous structure. In contrast to findings of Rahman et al.,[3,21] who reported a large effect of MW of PE on the growth and structure of TiO_2 composites, Kniprath et al. illustrated that the surface characteristics of PSS/TiO_2 NP or PDADMAC/TiO_2 NP films were independent of the MW of the PE.[5] They used MWs of 70 and 1000 kg mol^{-1} for PSS and $<$100 kg mol^{-1} and 400 to 500 kg mol^{-1} for PDADMAC. In these studies, only a couple of MWs have been considered, so it is hard to reach a conclusive picture of the effect of MW. Thus, there is need for further study of MW on the growth kinetics and surface morphology of PE/NP composite films.

In addition to the MW of the PE, the pH and salinity of the deposition solutions are decisive factors that affect the buildup of LbL films. The pH, for example, affects the charge density of weak PEs.[22] Bieker and Schönhoff investigated the effect of the pH of the depositing solutions on the growth of poly(allyl amine hydrochloride) (PAH)/poly(acrylic acid) (PAA) LbL assemblies.[23] They discovered various growth regimes with different growth behavior (linear and exponential) and film quality (soft and rigid) with simple variation of pH. They rationalized their observations by noting that, at different pH values, the degrees of ionization, electrostatic interactions, mobility, and interdiffusion of PE chains varied. Peng et al. studied the effect of pH and salinity of deposition solutions on the growth kinetics of PEI/SiO_2 NP composites, and showed that the deposition of low-pH SiO_2 NPs and high-pH PEI resulted in exponential film growth.[24] They claimed that the pH difference between PEI and SiO_2 solutions during LbL assembly altered the charge of PEI chains and thereby enhanced their diffusion, so that during a single NP deposition step, more NPs were able to be deposited, leading to deposition of multiple layers of SiO_2 NPs in a single deposition step.

Salt has two competing effects on the growth kinetics of LbL films. First, simple ions screen the electrostatic interactions and reduce the driving force for LbL assembly.[22] Second, salt-induced weakening of electrostatic interactions increases the diffusivity of polymer chains and affects their conformation. Recently, our group studied the effect of pH and salinity on the growth of PE/PE LbL films and how the growth rate correlated to the bulk complexation thermodynamics of the two PEs at the same pH and salinity.[22] It was shown that, although there was no one-to-one correlation between different regimes of LbL growth (linear and exponential growth) and bulk complexation (precipitate and coacervate formation), salinity influenced the growth kinetics in a more or less universal fashion. It was shown that growth rate increased with salinity at low salt concentration, whereas it decreased as the salt concentration approached the critical concentration for dissolution of the bulk polymer-rich phase into a single phase. It was demonstrated that, depending on the PEs employed, variation of pH and salinity could dramatically alter the growth mode of LbL films from linear to exponential and vice versa.

The effects of ionic strength of the deposition media on the growth rate of PE/NP composites have been studied as well.[5,24–28] Ghannoum et al. studied the growth kinetics of LbL assembly of PDADMAC and platinum NPs capped with poly(-acrylate), and showed that film growth was very sensitive to the ionic strength of the suspension.[25] They identified 50 mM as the optimum salt concentration beyond which film growth degraded. Some studies focused on the salinity of PE solutions because the addition of salt to particulate suspensions could lead to aggregation as electrostatic repulsion was screened. Peng et al. demonstrated that addition of salt to a PEI solution degraded the growth of PEI/SiO_2 NP films.[24] In contrast, Ostendorf et al. reported that increasing the ionic strength of PAH solution up to 1 M increased the thickness of PAH/gold NP films somewhat, although it did not seem to affect the amount of NPs deposited in the film.[26] Kniprath et al., on the other hand, found that increasing the ionic strength of the PE solution from 0 to 1 M did not affect the surface morphology of the resulting PSS/TiO_2 NP or PDADMAC/TiO_2 NP films.[5] All in all, it seems that the only clear conclusion that can be drawn is that the effect of salinity on the growth and structure of LbL films strongly depends on the specific chemistry of the ingredients.

Despite the importance of the observations made in previous studies, to the best of our knowledge, there has not been a systematic study of the effect of the MW of the PE on the growth kinetics of PE/organic NP LbL films. We therefore herein elucidate how MW affects the way growth kinetics varies with NP size and salinity of the media (both PE and PS solutions). We also investigate the surface morphology of LbL films with different MWs by using AFM and SEM. As a model for organic NPs, we chose polystyrene (PS) beads of different size and surface functionalization to study the growth kinetics of their LbL assembly with two different PEs, namely, PEI and PAA. As weakly dissociating PEs, PEI and PAA are selected, so that their charge density can be tuned with pH. Prior to studying the effect of MW, we examine the effect of NP concentration, the pH of the deposition solutions, and the deposition time to find the optimal growth conditions for each parameter. This study is aimed at engineering the structure of LbL films composed of organic NPs and PEs.

2. Results and Discussion

2.1. PEI/PS− System

Initially a multilayer system composed of positively charged PEI as the PE and negatively charged PS (PS− hereafter) NPs carrying strongly charged sulfate functional groups were chosen. The effects of deposition time, NP concentration, solution pH, and PEI MW on growth were studied. We show that variation of these parameters enables us to tune the growth kinetics of PEI/PS− composites. Results for the effect of deposition time on film buildup are shown in Figure S1 in the Supporting Information for brevity.

2.1.1. Effect of NP Concentration

Figure 1 indicates the effect of NP concentration on the growth kinetics of a PEI/PS− composite. As shown in this figure, for the same mass concentration of 0.1 wt%, smaller NPs (41 nm sized ones) lead to larger frequency shifts, and thus, greater mass depositions in the PEI/PS− film, which may seem counterintuitive. However, for the same mass concentration, larger NPs have a lower number density in solution than smaller ones do. Due to their much slower diffusion, it is therefore less likely for the larger NPs to be adsorbed into the PEI/PS− composite.

To find the proper basis for assessing particle concentration, the growth of films with 100 nm sized particles was studied at the same particle number density as that for 41 nm sized ones. A dense suspension of 100 nm sized particles with a concentration of 1.5 wt% (which has the same number density as a 0.1 wt% suspension of 41 nm particles) was therefore used in combination with a solution of PEI of the same concentration as before to grow PEI/PS− multilayers. In this case, the deposition rate of PS− NPs was so fast that the entire chrome/gold crystal was instantly coated by a visibly thick layer of NPs. At the same number density, the larger 100 nm particle suspension produces an LbL film with a frequency shift that is at least five times greater than that of the smaller 41 nm sized particles. Thus, there does not seem to be a clear choice for a concentration basis at which composite films of different NP sizes yield the same growth rate. Consequently, for simplicity, the rest of the experiments were performed with PS NPs of 0.1 wt% concentration. It is also evident from Figure 1 that, for the same NP size of 100 nm, increasing the suspension concentration boosts the growth kinetics of PEI/PS− thin films.

Finally, the data in Figure 1 indicates that PEI/PS− thin films grow through a cooperation between PEI and PS− deposition steps. More PEI deposited in an LbL step results in more PS− NPs being deposited in the subsequent step. Also, the "stepped" appearance of the growth or "odd–even" effect observed in Figure 1, with a relatively small mass added in the odd steps, shows that contribution of the PEs to the frequency shift is much less than that of the NPs. This trend was observable for all growth study experiments. This phenomenon has already been reported in the literature.[28]

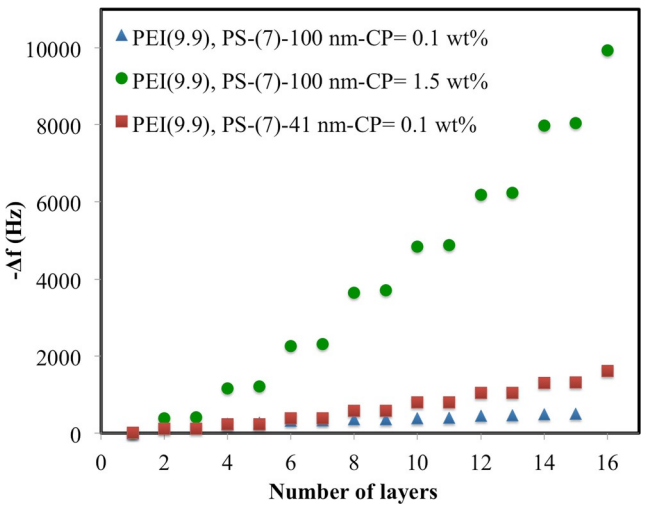

Figure 1. The effect of NP concentration and size on the growth kinetics of a PEI/PS− thin film. PS− NPs are deposited during even-numbered steps. PEI with a MW of 750 kg mol^{-1} is used. In the legend, the numbers in parentheses indicate the pH value of the solutions. For each case, the diameter of the employed NPs is given in nm. CP stands for concentration of particles. In this and all figures, the polymer monomer concentration used in the solutions is 0.23 M.

2.1.2. Effect of Solution pH

Figure 2 depicts the influence of pH on the buildup of PEI/PS− multilayers. PS− NPs are functionalized with sulfate groups, so their surface charge is independent of pH and they are stable over a wide range of pH. On the other hand, PEI is a weak PE ($pK_b \approx 10$[24]), the charge density of which is dependent on pH. At pH 9.9, PEI should be nearly 50% charged, whereas decreasing the pH to 7 renders PEI chains nearly fully charged. PS− NPs with a diameter of 41 nm were chosen because their diameter was an intermediate value among the group of PS− NPs studied herein.

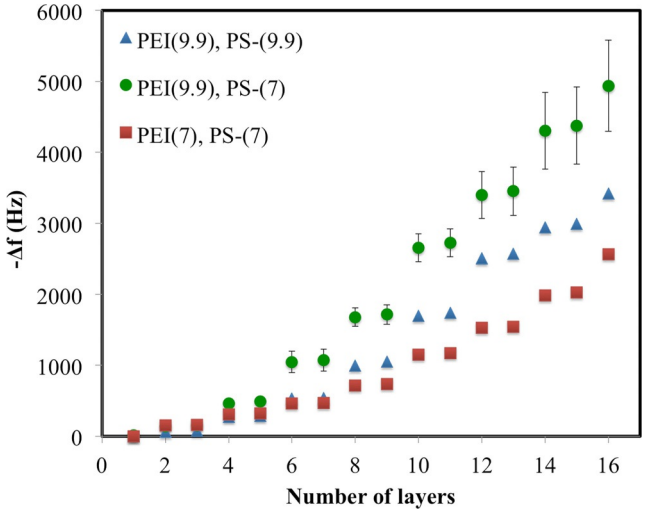

Figure 2. The effect of pH on LbL growth of a PEI/PS− composite. PEI with a MW of 70 kg mol^{-1} and 41 nm sized PS− particles are employed. The concentration of PS− NPs is 0.1 wt%.

As shown in Figure 2, the pH values of both the solution of PEI and PS− suspension have considerable influence on the growth kinetics of the PEI/PS− composite. Furthermore, the growth rate of the PEI/PS− film is fastest when solutions of PEI and PS− have pH values of 9.9 and 7, respectively.

The degree of ionization has a dramatic influence on the growth rate of a PEI/PS− composite. When PEI and negatively charged PS solutions are deposited at the same pH (=7.0), PEI chains are expected to be fully charged. When PEI chains are deposited at pH 9.9, however, their charge is less than it is at pH 7.0, and more chains need to deposit atop the underlying NPs to compensate for the opposite charge on the film. Based on the pK_b of PEI in the bulk, the charge density of PEI at pH 7 should be roughly twice as high as it is at pH 9.9. It should be noted, however, that weakly dissociating PEs of oppositely charged functional groups inside PE/PE multilayer films have long been shown to be more highly charged than those in solution as a result of the charge regulation effect.[29,30] The surface functional groups on PS− NPs can thus induce further charging in PEI chains at pH 9.9 once they are fully embedded in the film. However, since the growth is markedly faster for PEI chains deposited at pH 9.9 with PS− NPs at pH 7, compared with the other two conditions studied in Figure 2, the PEI chains deposited at pH 9.9 are likely to be far from being fully charged. Therefore, the PS− NPs need to absorb more PEI chains at pH 9.9 than they do at pH 7 to achieve charge compensation, leading to faster growth.

The degrees of charge compensation for three different LbL growth experiments studied herein are presented in Figure S2 in the Supporting Information. From the quartz crystal microbalance (QCM) data shown in Figure 2, we understand that the frequency shift ratio (or equivalently the mass per unit area ratio) of deposited NPs to that of PEs in each double layer is in the order of 10, whereas the charge compensation factor (defined as the ratio of charges associated with NPs to those of PEs) for each double layer for these experiments is in the order of only 0.01 (see Figure S2 in the Supporting Information); this indicates that the charges on the NPs deposited in a layer fall far below that needed to compensate for the charge on the PE layer deposited in the layer just beneath it. (We must here add the important caveat that the difference in total film mass between deposition of each layer is taken as a measure of the mass actually deposited from the solution. It is possible that the mass of NPs deposited is much greater than this, if an equivalent mass of PE is washed off the film as the NPs are deposited.) The lack of strong charge regulation can thus be rationalized by fewer encounters between neutral PEI repeat units with particle surface functional groups in PE/NP films than would be expected in PE/PE films assembled under similar conditions. The NPs evidently serve as a sufficiently thick spacer between two alternating PEI layers that render a continuous film buildup feasible, despite the very low charge compensation ratios observed. Such excess of charge on PE chains in conventional PE/PE LbL assembly is unsustainable owing to a huge electrostatic repulsion that would be created between narrowly spaced layers of PE present in excess. Evidently, in PE/NP deposition, accumulation of PE charge from one bilayer to the next is possible. This is an unusual feature that, to the best of our knowledge, is unique to PE/NP assemblies.

Upon deposition of NPs at pH 7 following PEI deposition at pH 9.9, the neutral primary amine groups absorb a proton from the solution as a result of the sudden pH drop; thus creating a sudden jump in areal charge density of the chains decorating the surface. The higher charge density of the PEI-covered surface requires more sulfate-functionalized PS NPs as compensation, compared with cases without the abrupt pH change. Consistently, PEI and PS− NPs deposited at the same pH, either both at 7 or both at 9.9, yield thinner films than when the solutions are deposited at the two different pH values considered (Figure 2). Such a sudden charging of PEI chains is lacking when the solutions are deposited at the same pH.

Moreover, the film growth benefits from the high diffusivity of PEI chains into the film during PEI deposition at pH 9.9 due to lower charge density of PEI chains, which should lead to weaker binding to PS− particles, and hence, faster diffusion.[22] The higher diffusivity of PEI chains at pH 9.9 is probably another reason for the faster growth kinetics of PEI/PS− composite at this pH compared with the case in which both solutions are deposited at pH 7, despite stronger electrostatic interactions in the latter case.

As discussed in the Experimental Section, the pH of the rinsing water and PS NP suspension drift during deposition. The result is that, when the PS particles and PE polymer are deposited at different pH values, nominally pH 7 for PS− and nominally pH 9.9 for PEI, the actual pH values differ less from each other as more layers are deposited. As shown in Figure S3 in the Supporting Information, when the pH values of the rinsing water and PS− suspension were constantly monitored and maintained at their initial values, film growth improved. This observation further bolsters our argument that a larger difference between pH values of deposition solutions and rinsing waters leads to faster LbL film buildup.

The effect of pH on the growth kinetics of PEI/PS− composites observed herein is similar to that observed by Peng et al. for the multilayer buildup of SiO_2 inorganic NPs and PEI.[24] Herein, we have shown that, although the interactions are not exactly the same, a similar trend holds.

2.1.3. Effect of MW

Figures 3–5 indicate the role of PEI MW on the growth kinetics of PEI/PS− composites for different NP sizes. The NP concentration is set to 0.1 wt%. Conspicuous in Figure 3 is the sawtooth growth behavior of the films involving the 26 nm PS− particles. It seems that some of the deposited PS− NPs are washed off of the film during the deposition of the PEI (odd-numbered steps). Some PEI must have been deposited during these steps to explain the continued growth of the film in subsequent steps. Moreover, Figure 3 indicates that, for 26 nm PS− particles, a higher MW of 750 kg mol^{-1} leads to a thicker PEI/PS− composite.

Figure 4 shows that, for the 41 nm PS− particles, the PEI/PS− LbL buildup is maximum at an intermediate PEI MW of

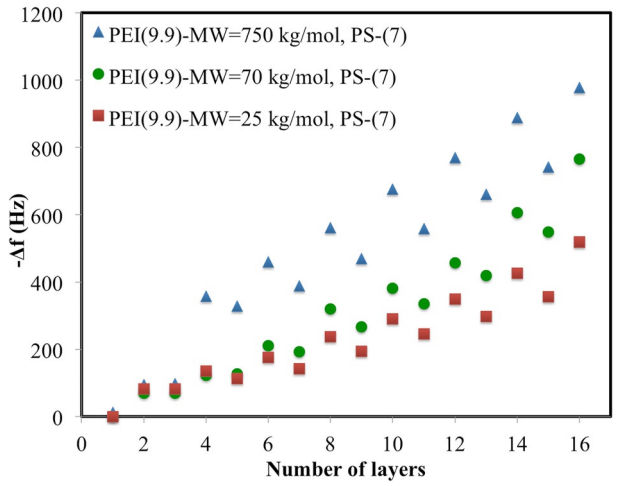

Figure 3. The role of the MW of PEI on the growth of PEI/PS− LbL film, for PS− NP sizes of 26 nm.

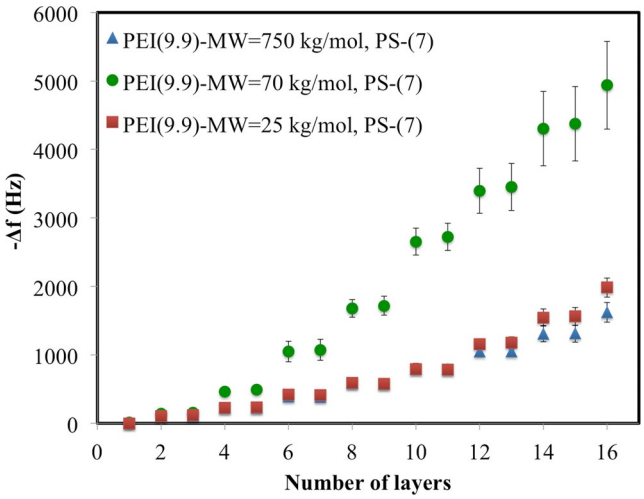

Figure 4. The role of the MW of PEI on the growth of PEI/PS− LbL film, for PS− NP sizes of 41 nm.

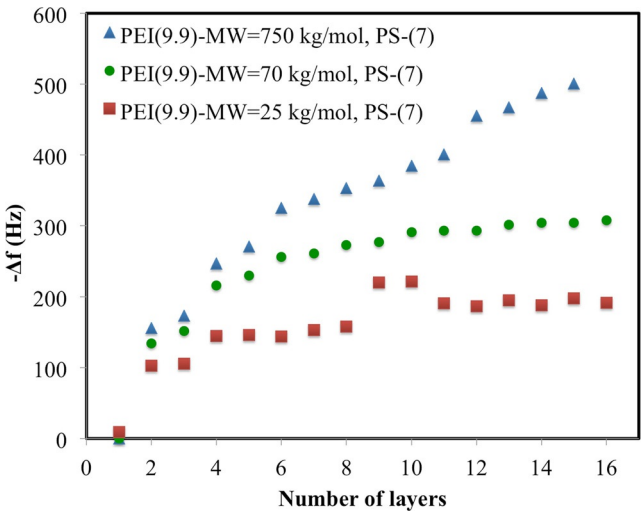

Figure 5. The role of the MW of PEI on the growth of PEI/PS− LbL film, for PS− NP sizes of 100 nm.

70 kg mol^{-1}. Also, unlike the growth kinetics of the 26 nm sized PS− particles, for 41 nm sized PS− particles, out diffusion of ingredients from the film is not observed. Moreover, all three data sets depicted in Figure 4 show accelerating, or "exponential", growth for the particle deposition steps, with increasing numbers of layers. This is especially noticeable for the PEI with a MW of 70 kg mol^{-1}.

According to the results shown in Figure 5, for 100 nm sized PS− particles, the PEI with the highest MW leads to the thickest film.

2.2. PAA/PS+ System

In the next set of experiments, another composite system composed of negatively charged PAA as the PE and positively charged PS (PS+ hereafter) NPs carrying amidine functional groups was selected. PAA is a weak PE ($pK_a \approx 5–5.5$[22]). It is approximately 50% charged at pH 5, and therefore, almost completely charged at pH 7.

If the PE/NP LbL growth were entirely driven by electrostatic interactions, it would be plausible to expect that switching the sign of charges on both components would not alter the trends. The LbL experiments with the PAA/PS+(amidine) system thus establish whether the trends observed for the effect of MW on the growth of PEI/PS−(sulfate) multilayers discussed in the previous section are general, that is, chemistry-independent. Similar to the PEI/PS− system, for the PAA/PS+ composite, increasing the PS+ concentration boosts the growth rate, as shown in Figure S4 in the Supporting Information.

2.2.1. *Effect of MW*

Figures 6–8 show the growth kinetics of PAA/PS+ LbL assemblies for different MWs of PAA and various NP sizes. Throughout this section, the concentration of PS+ NPs was set to

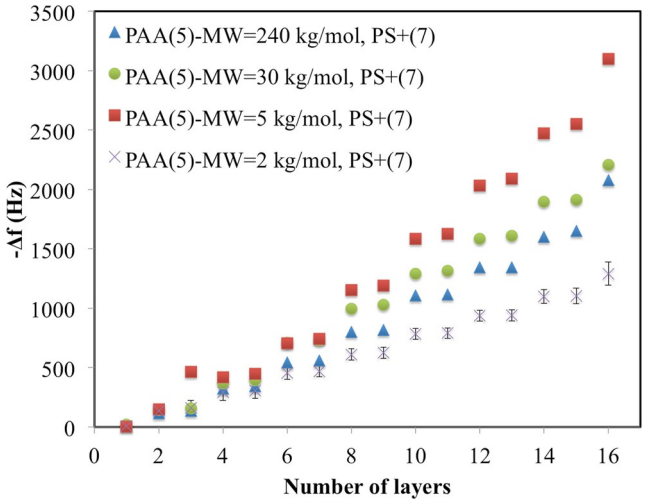

Figure 6. Effect of MW of PAA on PAA/PS+ LbL buildup with 23 nm sized PS+ particles. For this and subsequent figures, the pH values for each deposition solution (PAA or PS+) is indicated in parentheses. Notably, the value of error bars for PAA with MW of 2 kg mol^{-1} is small.

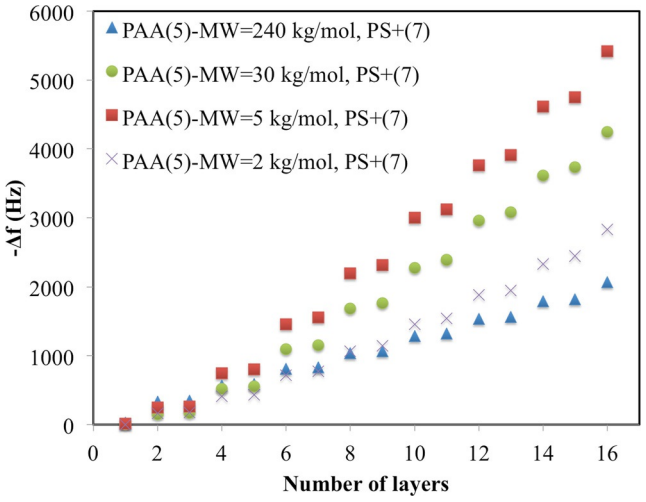

Figure 7. Effect of MW of PAA on PAA/PS+ LbL buildup with 44 nm sized PS+ particles. Data for PAA with a MW of 30 kg mol^{-1} have error bars, but these are too small to be visible.

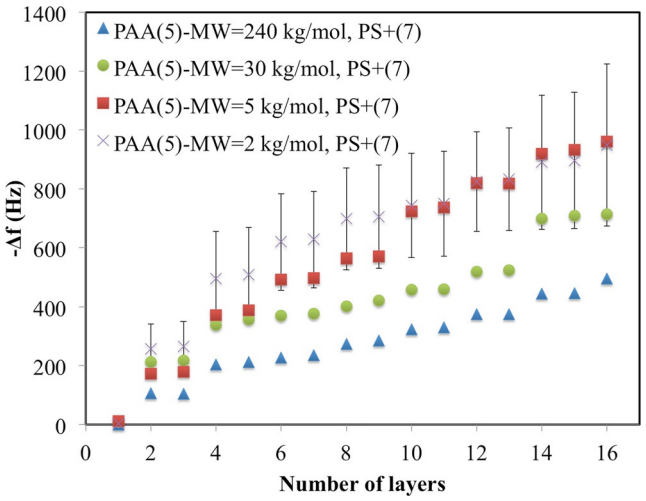

Figure 8. Effect of MW of PAA on PAA/PS+ LbL buildup with 100 nm sized PS+ particles.

0.1 wt%. Unlike the PEI/PS− system with 26 nm sized particles (Figure 3), out diffusion of the PS+ NPs of similar size, 23 nm, is not observed for the PAA/PS+ counterpart shown in Figure 6.

According to the results shown in Figures 6 and 7, the MW has a non-monotonic effect on the LbL buildup of PS+ particle of 23 and 44 nm in size. Decreasing the MW from 240 to 5 kg mol^{-1} boosts the LbL growth rate, but a further decrease in MW leads to a slower growth rate. Evidently, a further decrease in the MW to 2 kg mol^{-1} lowers the capability of chains to immobilize the PS+ NPs in the composite film. Therefore, there is an optimum MW for the growth of PAA/PS+ multilayers, which is 5 kg mol^{-1} for both 23 and 44 nm sized PS+ particles.

Given the margin of error in Figure 8, however, the growth of PAA and 100 nm sized NP film is virtually insensitive to a further decrease in MW from 5 to 2 kg mol^{-1}. We speculate that, similar to the behavior of the PS+ NPs of 23 and 44 nm in size, for 100 nm particles there should be an intermediate MW that leads to the fastest growth of PAA/PS+ films, although the optimal MW in the case of 100 nm sized NPs is less than or equal to 2 kg mol^{-1}. Given that it is impossible to use acrylic acid monomers as building blocks in LbL assembly, one would intuitively expect there to be an optimum MW less than or equal to 2 kg mol^{-1} for 100 nm sized PS+ NPs.

Table 1 summarizes the optimum growth behavior for the different NP sizes and PE MWs studied. For both PAA/PS+ composites with either 23 or 44 nm sized particles (Figures 6 and 7), and for PEI/PS− thin films with 41 nm sized particles (Figure 4), there is an intermediate MW that leads to the fastest LbL growth. However, the growth rate of PEI/PS− multilayers with 26 and 100 nm sized particles does not show an optimal MW over the range of MWs considered (Figures 3 and 5). Consequently, one can conclude that the effect of MW on growth kinetics of PE/NP thin films strongly depends on the specific chemistry of the ingredients, as well as on the size of NPs employed. We should also note that the surface charge density of the sulfate-functionalized particles (PS−) used to grow PEI films varies greatly with particle size, whereas the amidine-charged particles (PS+) have nearly the same charge density for all three particle sizes; this may also play a role in the different behavior observed for the two systems. Furthermore, as mentioned in the Experimental Section, PEIs had greater polydispersity indices than those of PAAs. This could also contribute to the different growth kinetics seen for the two systems studied. Although it is beyond the scope of the current study, the polydispersity of the polymer solutions employed could have a considerable effect on the growth behavior and is worth future investigation.

Chain diffusion, particle and chain redissolution, specific chemistry involved in the complexation of opposite charges, surface overcompensation, and interparticle bridging are some of the major factors, the relative influence of which control the overall LbL growth rate. MW, in particular, affects each of these factors in different and even opposite ways. For instance, chain diffusion is enhanced, whereas interparticle bridging is adversely impacted, as MW decreases. Our results demonstrate that flipping the sign of the charges borne by PEs and NPs leads to two distinct trends in the dependence of LbL growth on MW.

Table 1. Optimum LbL buildup for different PE/NP composites studied as a function of NP size and MW of PE.

PEI/PS− NP multilayers		PAA/PS+ NP multilayers	
NP size	Optimum MW	NP size	Optimum MW
26	large (750 kg mol^{-1})	23	intermediate (5 kg mol^{-1})
41	intermediate (70 kg mol^{-1})	44	intermediate (5 kg mol^{-1})
100	large (750 kg mol^{-1})	100	intermediate (2 and 5 kg mol^{-1})

For neutral polymers, the self-diffusivity decreases as the MW increases.[31] Decreasing the MW of the PE under otherwise identical conditions therefore increases the effective chain diffusivity, which tends to increase chain deposition into the film. On the other hand, we speculate that each deposited PE layer bridges the former and subsequent NP deposits. Longer chains can bridge the NPs more easily and chain entanglement would strengthen such interparticle bridges, boosting the film mechanical integrity. A trade-off between chain diffusivity and bridging could explain the intermediate optimum MW found for PEI/PS− composites with 41 nm sized PS− particles, as well as PAA/PS+ LbL films. However, the reverse trend is observed for two of the particle sizes employed in the PEI/PS− system (Table 1), for which, with 26 nm sized particles, appreciable redissolution appears to control the deposition rate (Figure 3). During chain deposition, the film surface charges arising from sulfate groups are compensated for by the amine groups along PEI chains. The incoming chains generally overcompensate for the surface charges, which reverses the sign of the surface charge. Longer chains have been shown to lead to greater charge overcompensation.[32] Although better charge overcompensation for the PEI with the highest MW can explain the deviation from the observed trend for the PAA/PS+ NP system, further detailed experimental techniques are needed to definitively elucidate this observation and better understand the underlying physics. It might be possible, for example, to use confocal laser scanning microscopy or neutron reflectometry to track the diffusion of polymer in the LbL film; this could shed light on the reasons for different growth behavior.[33] Also, single-molecule force spectroscopy experiments could be performed, wherein a polymer chain is detached from the film and the detachment force profile is measured. This is a useful method to determine polymer chain adhesion forces in films.[34]

For larger PS NPs, it is more difficult for PEs to create interparticle bridges and LbL films become unstable in this case. Interparticle bridging becomes even more difficult for shorter PE chains. This might be the reason for the larger error bars observed in Figure 8.

2.2.2. Effect of Salinity

Salt screens the electrostatic interactions between charged functional groups and also impacts the PE diffusivity in the multilayer film. The effect of the salinity of the deposition solutions for PAA/PS+ films composed of 44 nm sized PS+ particles and PAA with MWs of 5 and 240 kg mol^{-1} are shown in Figures 9 and 10, respectively. PS+ NPs with diameter of 44 nm were chosen because this size was an intermediate NP size among different PS+ NP sizes studied. According to the results in Figure 7, for this NP size, PAA with MWs of 5 and 240 kg mol^{-1} showed the fastest and slowest growth rates, respectively. We therefore chose these MWs to study the effect of salinity for both fast- and slow-growing films. For the PS+ suspension, even a salt content of 100 mM did not compromise the suspension stability, as verified by dynamic light scattering.

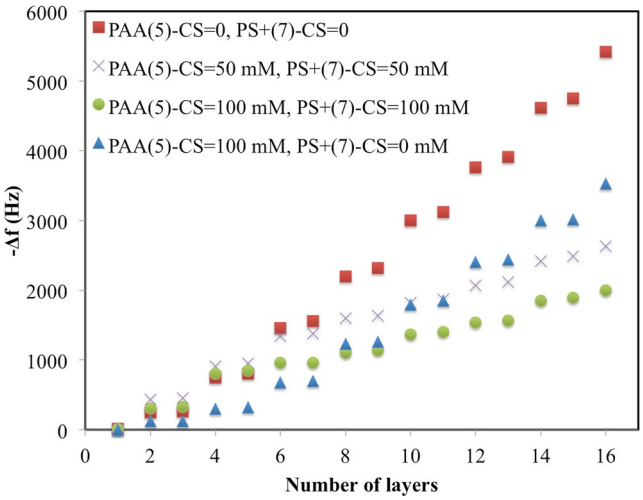

Figure 9. The effect of KCl concentration on the growth kinetics of PAA/PS+ multilayers for PAA with a MW of 5 kg mol^{-1} and 44 nm sized PS+ particles. The concentration of NPs was 0.1 wt%. The concentrations of salt (CS) in the PAA and PS+ solutions are shown in the legend. The ionic strengths were 37, 93, and 147 mM for PAA solutions with salt concentrations of 0, 50, and 100 mM, respectively. For PS+ suspensions, however, pH adjustment did not change the ionic strength of the suspensions. Thus, the ionic strength values were the same as the salt concentration reported.

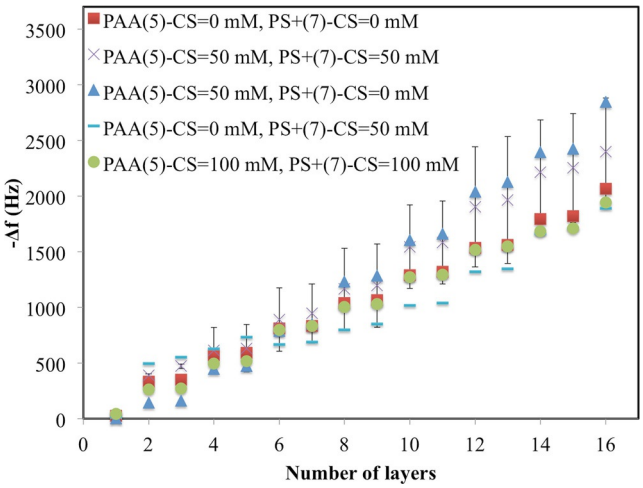

Figure 10. The effect of KCl concentration on the growth kinetics of PAA/PS+ multilayers for PAA with a MW of 240 kg mol^{-1}. The concentration of PS+ NPs was set to 0.1 wt%. The ionic strengths for PS+ suspensions with salt contents of 0, 50, and 100 mM were 0, 50, and 100 mM, respectively. Also, the ionic strengths of PE solutions with salt concentrations of 0, 50, and 100 mM were 34, 92, and 149 mM, respectively.

It should be noted that the pH of PE and PS solutions were adjusted by the addition of KOH and HCl for different cases studied. This introduced additional K^+ and Cl^- ions into the solutions on top of those introduced by adding KCl. In this section, the term "salinity" refers to K^+ and/or Cl^- added to the solutions through KCl salt, and does not include any ions contained in the pH buffer, KOH or HCl. To enhance clarity, the values of ionic strength of the deposition solutions (considering both ions introduced by addition of salt as well as pH buf-

fers) are reported in the captions of Figures 9 and 10. For the case of PS+ NPs, the concentration of ions added to the system for pH adjustment was far lower than the amount of K^+ and Cl^- ions added to the system to study salinity, so their effect on ionic strength was negligible. For PAAs, however, this was not the case. For the PAAs, higher salt concentrations (KCl) resulted in greater concentrations of K^- ions needed for pH adjustment. All in all, PAA solutions with higher salt contents needed more ions for pH adjustment, too.

As shown in Figure 9, the addition of KCl to a solution of PAA with a MW of 5 kg mol^{-1} has a detrimental effect on the buildup of the PAA/PS+ composite film; the growth rate decreases when 50 mM salt is added to both PAA and PS+ solutions, and a further decrease when the salt concentration is increased to 100 mM. Also, introducing KCl to the PAA solution only leads to a weaker degradation than when it is added to both solutions. Finally, the results in Figure 9 also demonstrate that, with the addition of KCl, composite films still grow linearly.

The effect of salinity on the growth rate of multilayer films composed of PAA (MW = 240 kg mol^{-1}) and PS+ NPs (44 nm in size) is indicated in Figure 10. This figure shows that for PAA with a MW of 240 kg mol^{-1}, the addition of KCl to both PAA and PS+ solutions or to a solution of PAA alone boosts the LbL growth kinetics. However, LbL growth is slightly degraded when KCl is only introduced into the PS+ suspension.

Figure 10 also illustrates that increasing the salt concentration from 50 to 100 mM decreases the growth rate of the PAA/PS+ composite film for PAA with a MW of 240 kg mol^{-1}. Comparing Figures 9 and 10, one can clearly observe that the salinity of the medium has a stronger effect on frequency shifts of PAA/PS+ films for the smaller MW of 5 kg mol^{-1} than that for a MW of 240 kg mol^{-1}. The largest MW of 240 kg mol^{-1} of PAA was investigated herein because for much higher MW values the higher viscosity made it practically impossible to study the film growth kinetics.

Although in the results presented herein the PEs interact with surface-functionalized NPs rather than with other polymers, as is the case for ordinary PE/PE deposition, the key interactions in both cases are electrostatic, and can be screened by mobile salt ions. In both cases, increasing the ionic strength decreases the thermodynamic driving force for complexation of PE and NP functional groups, and enhances the diffusivity of PE chains inside the films; this competition has been shown to affect PE/PE multilayer formation profoundly.[22] Which of these two factors is dominant thus determines whether the film growth is enhanced or degraded by the addition of salt. The relative importance of these two factors in the present study is affected by the MW of the PE. The diffusivity of the PE with low MW is already so high that salt should have only a marginal effect on chain diffusivity. Consequently, for low MW PEs, the reduction of the driving force is the dominant factor, which progressively slows down the growth kinetics of low MW PAA/PS+ NP composites as the salt concentration increases (Figure 9). Interestingly, adding salt only during PAA deposition (while using a salt-free NP suspension) leads to an intermediate growth rate.

For the PE with a higher MW, the boost in diffusivity due to the addition of salt apparently outweighs the reduced electrostatic attraction between the oppositely charged components, for salt concentrations up to 50 mM KCl, leading to a boost to LbL growth rate visible in Figure 10. However, a further increase in salt concentration from 50 to 100 mM and consequent reduction in the electrostatic driving force degrades the growth kinetics of PAA/PS+ composite. Unlike PEs, the deposition of NPs in Figure 10 is weakly affected by KCl, whereas changing the salt concentration in the PAA solution, while holding that of the NP dispersion fixed, appreciably alters the growth kinetics. In contrast to spherical NPs, PE chain conformation, thermodynamics, and diffusivity are all drastically altered by the ionic strength of the media and LbL growth rate is thus more sensitive to the salinity of the PAA solution than to that of the NP dispersion.

2.3. Film Characterization

2.3.1. AFM Study

To study the surface morphology, PEI/PS− composites with 41 nm sized PS− particles were selected. These composites are similar to most of the cases studied in that the intermediate value of MW leads to the fastest growth rate (Figure 4). Other than ions added to the solutions for pH adjustment, no extra salt ions were added to either of the ingredients for the LbL buildup. Furthermore, PEI and PS− solutions were deposited at pH values of 9.9 and 7, respectively. Figure 11 depicts surface characteristics of composites with different PEI MWs. Instead of performing localized AFM on a very small area, which is a common practice in the literature, a larger area (30 μm × 30 μm) was studied to obtain a more representative assessment of the surface morphology. As mentioned in the Experimental Section, eight different areas of each sample were imaged, but a single image most typical in the range of roughness for each sample is shown in Figure 11. The inset for each AFM image in Figure 11 is the same image as that in the corresponding main figure, except with the color scale bar fixed to a range of 700 nm, whereas in the main figures the scale bars are adjusted to keep the contrast fixed. Thus, the insets in Figure 11 allow one to compare the uniformity of roughness from sample to sample, with a uniform color and darkness indicating a film with relatively uniform roughness. The thin films, comprising a few layers, are uniformly dark in the insets because there can be little height variation on a scale of 700 nm when the films are much thinner than 700 nm. The main figures, with variable scale bars and fixed contrast, allow one to observe the surface topology, and the variation in height can be assessed for each figure from the corresponding color scale bar.

As can be seen in Figure 11, surface roughness during the growth of LbL films increases dramatically. This trend is seen for all PEIs with different MWs. Some studies have mentioned that LbL growth under pH-amplified conditions, that is, deposition of film ingredients at different pH values, could lead to rougher surfaces.[18] We tested the effect of pH-amplified depo-

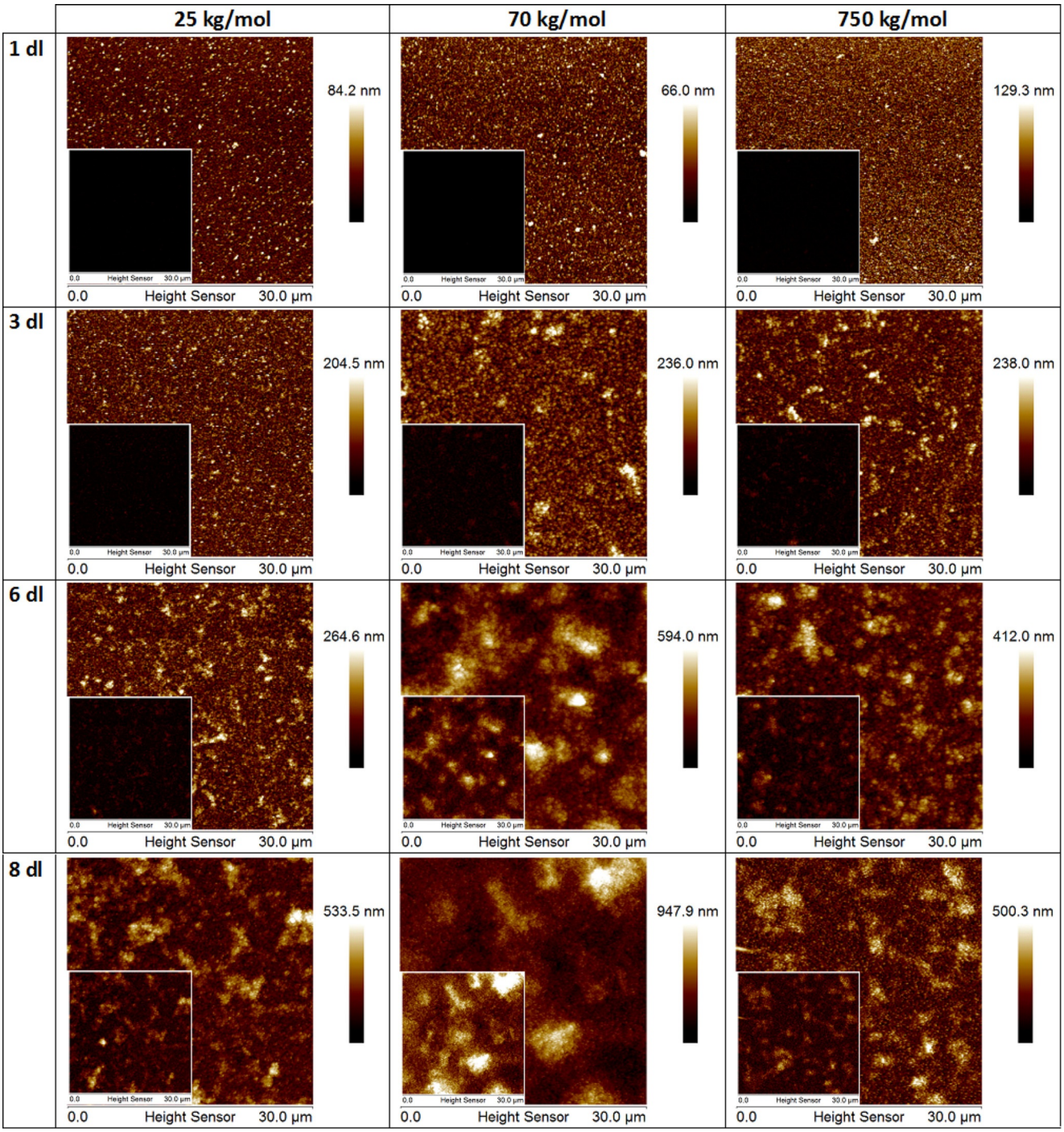

Figure 11. AFM images of PEI/PS− composites with 41 nm sized PS− particles and different MWs of PEI for different numbers of layers. All the images were obtained once PS− NPs are deposited for 1st, 3rd, 6th, and 8th double layers. The pH values for the NP and PEI deposition steps were 7, and 9.9, respectively. No salt ions were added for the growth of these films except for the ions introduced to the system to adjust the pH. The scale bars for the main images are also shown. The insets show the corresponding images rendered using a fixed 700 nm scale bar to allow comparison of film height uniformity on an absolute scale.

sition on the surface morphology of LbL films by first depositing 8 bilayers of PEI and PS− at pH values of 9.9 and 7, respectively, and contrasting these results with those obtained by depositing the same number of layers of PEI and PS− solutions both at pH 7. Root-mean-squared (rms) roughness values of the film surface were determined by examining the results with Nanoscope Analysis software (Bruker Nano, Inc.). AFM micrographs (Figure S5 in the Supporting Information) show that in the latter case (equal pH), the rms surface roughness is around 32% smaller than that in the former (unequal pH). However, because the two cases produced differing total film thicknesses, and roughness generally increases with thickness (Figure 11), rather than comparing the surface roughness for a fixed number of layers, the roughness-to-thickness ratio is

a better basis for comparison, since normally one wants to achieve a layer of a given thickness. Due to much slower growth of PEI/PS− composite when both PEI and PS− solutions are deposited at pH 7, in this case, the ratio of roughness to thickness is around 30% higher than that under pH-amplified deposition conditions. So, it seems that the amplification of LbL growth by using different pH values for different layers does not increase roughness, at least when roughness is normalized by film thickness. Another possible reason for the high surface roughness could be an uneven distribution of surface charge on the crystal surface, despite the fact that we were careful to be consistent when treating the substrates with piranha solution.

Figure 12 depicts the variation of both absolute roughness (shown in the inset) and roughness normalized by the film thickness for PEI/PS− thin films with different PEI MWs. Average film thicknesses of PEI/PS− films composed of PEI with MWs of 25, 70, and 750 kg mol^{-1} were estimated to be 330, 825, and 270 nm, respectively. These estimations were obtained by converting the frequency shift (data in Figure 4) of the QCM measurements to mass per unit area by using the Sauerbrey equation [Eq. (1) shown in the Experimental Section]. Knowing the mass per unit area and the density of film ingredients, one can estimate average film thickness. Because of the much greater mass deposition of NPs than of PEs, the density of the PS (1.05 g cm^{-3}) is used to convert the mass of film into thickness. Thus, the effect of the small density difference between the PS and PEs is neglected. This makes calculations much easier and generates minimal error (≈0.3% in the worst case) in the final results.

Figure 12 shows that, regardless of the MW of the PEI, as more layers are deposited onto the films, the ratio of roughness to thickness decreases, while the absolute roughness increases. Furthermore, Figure 12 shows that PEI with intermediate MW has the smallest roughness to thickness ratio, perhaps due to the fast growth of its thickness. As can be seen in the inset of Figure 12, LbL films composed of PEI with MWs of 25 and 750 kg mol^{-1} have comparable roughness values. Interestingly, these films had a similar rate of multilayer buildup (Figure 4).

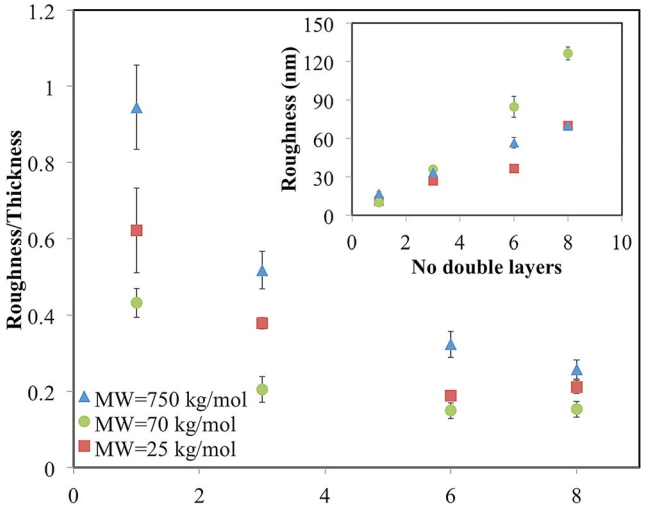

Figure 12. Ratio of roughness to thickness, extracted from AFM images, for the PEI/PS− multilayers depicted in Figure 11. The inset shows the variation of absolute roughness. For some data points, the error bar is too small to be visible.

2.3.2. SEM Study

2.3.2.1. Effect of MW

Figure 13 shows SEM images of the surfaces of LbL films with different MWs of PEI, grown with the same materials and under the same conditions as those used for the AFM images in Figure 11. At least five different regions of the samples were randomly selected to obtain micrographs with magnifications of 400. Those chosen for Figure 13 represent the typical features observed in the images. For micrographs with a magnification of 80 000, however, only three different parts of the samples were imaged, since different micrographs looked very similar to each other at this magnification.

Figure 13 shows that the PEI/PS− multilayer film composed of PEI with MW of 70 kg mol^{-1} has a more heterogeneous surface than those of the films for the other two MWs studied, which is consistent with the AFM results.

2.3.2.2. Thick Film Growth

PEI with a MW of 70 kg mol^{-1} and 41 nm sized PS− particles led to the thickest LbL film among different PEI/PS− composites studied in the previous sections. Thus, for this multilayer film, the LbL growth was continued until 59 double layers of PEI/PS− NPs were deposited on the glass substrate. Then, the surface morphology and thickness of the film were studied. Figure 14 depicts the characteristics of such a composite observed by SEM. As can be seen in the surface micrograph (Figure 14a), the glass slide is completely covered by the film ingredients. There were some cracks and uneven features noticeable on the surface of the film, however. Comparing the insets of Figures 13 and 14a, we see more dark regions in the latter, possibly indicating that the films are more disorganized and particles are more aggregated for the thicker film shown in Figure 14a. Moreover, Figure 14b shows that a relatively thick film with a thickness of a few microns is deposited on the substrate. Film thickness was not uniform throughout the cross section and could have drastic variations. To be able to perform SEM on the film cross section, the substrate was broken. As can be seen in Figure 14b, the film cross section is slightly scratched as a result of breaking the glass slide.

3. Conclusions

We studied the effect of MW of PEs, type and charge of PE, NP size, pH, and salinity on the growth kinetics of PE/organic NP multilayer films. First, we found that we could not deposit oppositely charged NPs alternately on top of each other in a manner that could survive rinsing steps, unless there were intervening PE layers. This showed that the PE and its binding

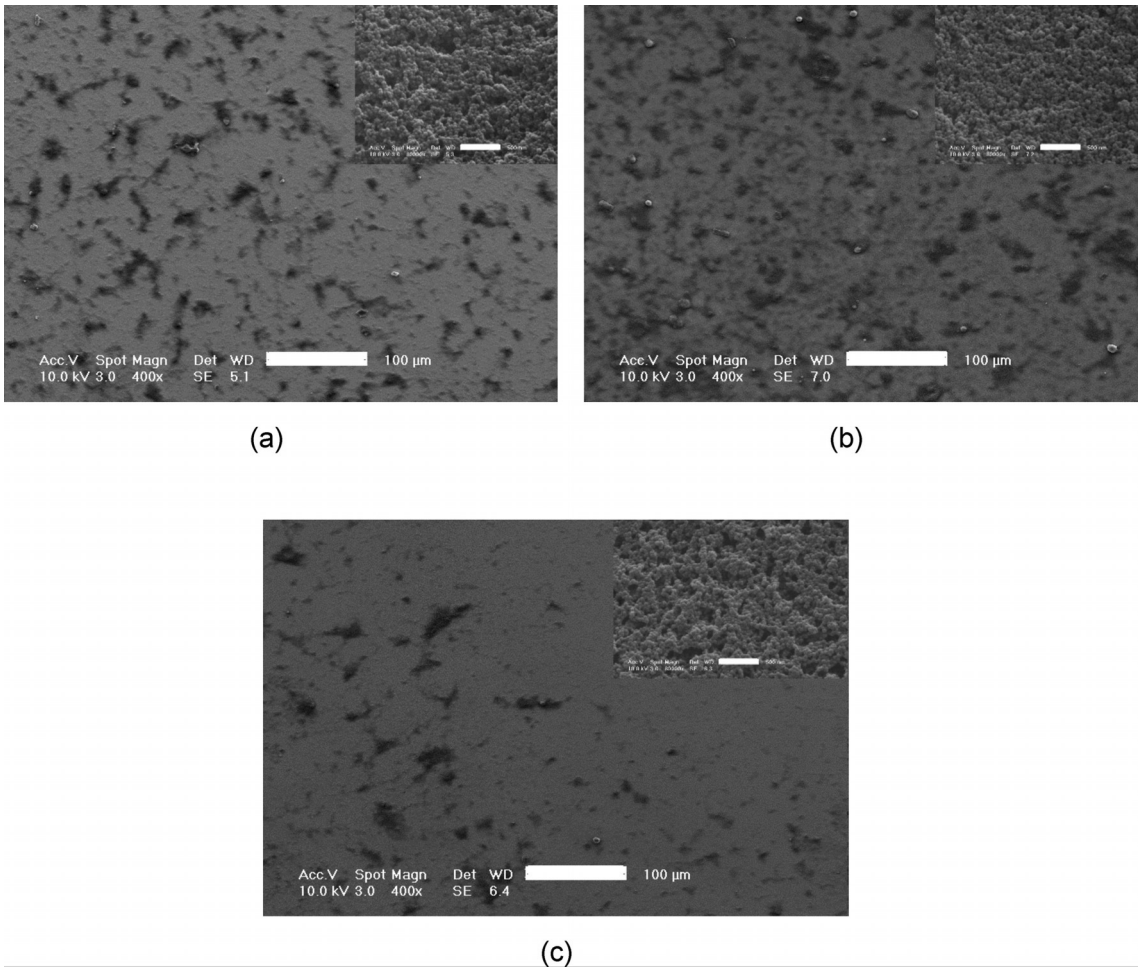

Figure 13. Surface morphology of LbL films composed of 8 double layers of PEI and PS−, with the same materials and under the same conditions as those used for Figure 11, with PEI MWs of 25 (a), 70 (b), and 750 kg mol^{-1} (c). The main figures have a magnification of 400, whereas the insets have a magnification of 80 000. The scale bars represent a length of 100 µm in the main figures, whereas those of insets indicate a length of 500 nm.

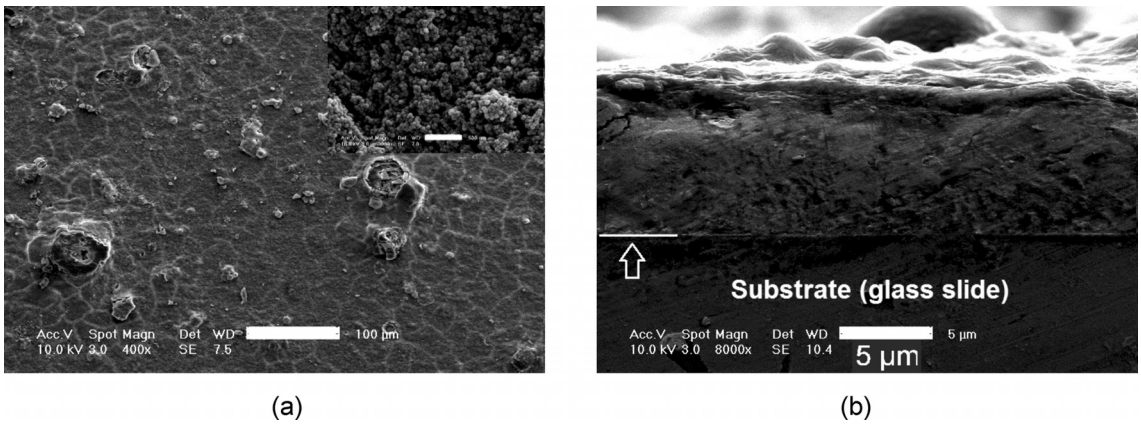

Figure 14. Characteristics of LbL film composed of 59 double layers of PEI and PS− NPs, with a PEI MW of 70 kg mol^{-1}. PEI and PS− solutions were deposited at pH values of 9.9 and 7, respectively. No salt was used in either of the film ingredients, except for the addition of HCl or KOH for pH adjustment. a) Surface of the film with a magnification of 400 in the main figure and 80 000 in the inset. The scale bars show a length of 100 µm for the main figure and 500 nm for the inset. b) Cross-sectional view of the film with a magnification of 8000. The arrow indicates the interface between the substrate and film.

and bridging of NPs was an essential mechanism for LbL film growth involving NPs. We showed that, for both cationic PEI deposited alternately with anionic PS (PS−) NPs and for anionic PAA deposited alternately with cationic PS (PS+) NPs, an intermediate value of MW could (with some exceptions) lead to the fastest film buildup. This behavior could be explained as

a trade-off between faster diffusivity for smaller chains during the deposition step at the expense of weaker adhesion and washing off of particles during the deposition or rinse steps when the MW became too low. However, for films composed of PEI with 26 or 100 nm sized particles, the PEI with the highest MW led to the thickest film.

The pH of PEI and PS− solutions had a dramatic influence on the LbL growth; in general, reducing the charge on the PEI by depositing it at higher pH caused greater deposition of PEI and of subsequent layers of PEI and NPs. In particular, fast film growth was obtained by depositing PEI at pH 9.9 and oppositely charged PS− NPs at pH 7.0. We showed that salinity affected the growth kinetics of LbL films differently, depending on MW of the PE. For low MW PEs, increasing the salt concentration decreased the film growth rate monotonically, whereas for higher MW PE addition of salt first improved and then degraded the multilayer buildup.

Some of these trends, especially the effects of pH and PE MW and, to some extent, the effect of salinity, could be understood qualitatively, but even the general trends observed were defied for some particle sizes, depending on the particular PE. Even when the expected trend was followed, for example, the non-monotonic dependence of growth rate on PE MW, the value of the optimal MW varied greatly (more than an order of magnitude) from PEI to PAA, for no reason we could determine. Hence, although some qualitative trends are now evident and explicable, even semiquantitative predictions are not yet in sight, and there are polymer-specific exceptions to even the qualitative trends.

Clearly, much progress is still needed to develop an improved qualitative and quantitative understanding of LbL deposition of PEs and NPs. In addition to further systematic LbL growth experiments, such as those performed herein, more detailed microscopy experiments could be very helpful. These experiments could include AFM studies of binding and adhesion forces between individual NPs and PEs, direct measurements of PE and NP diffusion in the film, fluorescence resonance energy transfer (FRET) measurements of binding and unbinding events, and other direct measurements of molecular structures and transitions. Applications of these methods to drug delivery and other applications can be pursued, based in part on the film-growth optimization results and methods presented herein.

Experimental Section

Materials

PEI and PAA with different MWs were employed as the polycation and polyanion, respectively. Branched PEI with MWs of 750 [polydispersity index (PDI): 12.5] and 25 kg mol^{-1} (PDI: 2.5) were purchased from Sigma–Aldrich (St. Louis, MO). Branched PEI with a MW of 70 kg mol^{-1} (PDI: 13) and PAA with MWs of 2, 5, and 30 kg mol^{-1} (PDI for these polymers: 2.4) were purchased from Polysciences (Warrington, PA). PAA with a MW of 240 kg mol^{-1} was obtained from Acros Organics (Belgium). The PDIs were obtained from the manufacturers.[35] Negatively charged PS (PS−) NPs with sulfate functional groups with particle sizes (diameters) of (26 ± 3), (41 ± 6), and (100 ± 8) nm, as well as positively charged PS (PS+) NPs with amidine functionalization and particle sizes of (23 ± 5), (44 ± 6), and (100 ± 9) nm were purchased from Life Technologies (Eugene, OR). The sulfate-functionalized NPs (PS−) with sizes of 26, 41, and 100 nm had highly varying surface charge densities of 3.4, 0.6, and 0.2 μC cm^{-2}, respectively. On the other hand, NPs containing amidine functionalization (PS+) with sizes of 23, 44, and 100 nm had nearly the same surface charge densities of 3.0, 3.4, and 3.2 μC cm^{-2}, respectively. The surface charge densities and particle sizes were obtained from the manufacturer.[35] KCl was obtained from Sigma Aldrich to study the effect of salinity on LbL growth. All other materials were purchased from Sigma Aldrich. No additional purifications were performed on the materials.

QCM Measurements

The growth of PE/NP multilayers deposited on quartz crystals was monitored under dry conditions with a QCM (QCM-200, Stanford Research Systems Inc., Sunnyvale, CA). Chrome-/gold-coated quartz crystals were obtained from Stanford Research Systems and had a resonance frequency of around 5 MHz. Initially, crystals were treated with piranha solution (a mixture of sulfuric acid and 30% hydrogen peroxide; 3:1 v/v) for 2.5 min. ***Warning!*** Piranha solution is very reactive and dangerous and considerable care should be taken when handling it. Piranha treatment not only cleaned the substrate, but it also made it negatively charged. Such a negatively charged substrate was needed for the subsequent PE deposition step. Next, the crystals were rinsed thoroughly with deionized (DI) water and dried with a flow of air. HPLC water (Fisher Scientific, Waltham, MA) was used for preparing PE or PS solutions. PE solutions employed in this research all had the same monomer concentration of 0.23 M. PS suspensions were used at a concentration of 0.1 wt%, unless specified otherwise. PS suspensions were sonicated with a probe sonicator (Ultrasonic Processor, Cole-Parmer Inc., Vernon Hills, IL) for 33 s prior to use to avoid agglomeration of NPs. To adjust the pH value of the PE/PS solutions, HCl and KOH were used and pH values were measured with an Orion 3Star Benchtop pH and conductivity meter (Thermo Scientific). In each plot in the Results and Discussion section, the pH for each solution used during multilayer growth was expressed in parentheses. The pH of deposition solutions was adjusted at the beginning of the LbL growth experiments. We found that for rinsing waters and NP suspensions the pH drifted over time. For the case of rinsing water and NP suspension at pH 7, pH drift was not significant and was typically below 0.5 units. However, for rinsing water with pH 9.9, the variation in pH could be larger (even more than 1 pH unit). A similar pH variation during LbL growth was reported by Peng et al.[24] In Figure S3 in the Supporting Information, we have compared the effect of pH drift on LbL growth. We believe that such drift does not have a significant influence on the trend of the results because all of the experiments were performed under similar conditions and time durations. For the PE solution, pH drift was not found to be an issue because the pH was stable over several days.

To commence LbL growth, the PE solution was poured onto the crystal surface and was left there for 15 min, unless specified otherwise. Subsequently, by using DI water with the pH of the deposition solution, the crystal was rinsed to remove excess PE chains that were not attached to the surface electrostatically. Next, the crystal was dried under a gentle flow of air. Afterwards, the variation in vibration frequency was recorded by using the QCM. Subsequently, the abovementioned procedure was repeated for the PS suspension to deposit a PS layer on top of the deposited PE layer.

The deposition of PE/PS layers was continued until eight bilayers were grown on the quartz substrate.

As mentioned before, the resonance frequency shifts of the chrome/gold crystal oscillator were recorded after each deposition step in each experiment. According to the Sauerbrey equation for rigid films,[24,36,37] the deposited mass per unit area (or thickness) is linearly related to the shift in resonance frequency, as shown in Equation (1):

$$\Delta f = -C(\Delta m) \quad (1)$$

in which Δf is variation of vibration frequency of the QCM crystal; Δm represents the deposited mass per unit area; and C is the crystal sensitivity factor, which is 56.6 Hz cm^2 μg^{-1} for the chrome-/gold-coated quartz crystals, as reported by the manufacturer.[37]

Prior to the growth of a PAA/PS+ composite, a layer of PEI with a MW of 750 kg mol^{-1} and pH 7 was deposited onto the substrate as the precursor, or primer layer. However, PEI/PS− multilayers were directly grown on the crystal without needing a precursor layer. All experiments were performed at room temperature of (22±3) °C. It should be noted that in all the plots shown in the Results and Discussion section, odd- and even-numbered steps represented PE and PS depositions, respectively.

Growing Thick Multilayer Films

To grow films of several LBL-assembled PE/PS double layers, an LbL robot (StratoSequence, nanoStrata, Inc., Tallahassee, FL) was used. The films were grown by dipping a microscope glass slide (Fisher Scientific, Waltham, MA) into PE/PS solutions for 10 min. For QCM experiments, a deposition time of 15 min was used. We studied the effect of deposition time on LbL growth by using a QCM and found that there was negligible variation in film growth for deposition times between 10 and 15 min (results shown in Figure S1 in the Supporting Information). Thus, we chose a 10 min deposition time for growing very thick films with the robot to reduce LBL buildup time, while ensuring maximum film growth. After each deposition step, the glass slides were dipped successively into two beakers containing DI water with the pH set to the same as that in the preceding deposition solution. Subsequent to the rinsing steps, the film was blown dry with a flow of air for 3 min. The film buildup was continued until 59 double layers of PE/PS were deposited onto the surface. The glass slide was treated with piranha solution prior to film growth. The amount of each dipping solution was constantly monitored to ensure that the solution volume remained at nearly 120 mL throughout the experiments. The PS suspension was sonicated each time considerable agglomeration of NPs was seen due to dipping of the glass slide and possible complexation formation of free NPs with film ingredients. Fresh particle suspensions used for thick multilayer growth looked clear. When the PS suspension seemed too cloudy and contaminated by multiple dipping steps, the entire suspension was changed for a fresh one. For the PE solution, however, no noticeable change in solution quality was observable after the dipping steps. Nevertheless, as a precaution, the PE solution was changed after every 20-bilayer buildup, or so. Furthermore, the rinsing waters were changed with fresh ones after every four double-layer growth steps.

AFM Studies

An atomic force microscope (Dimension Icon, Bruker Nano Inc., Santa Barbara, CA) was employed to study the surface morphology of the films during LbL growth. AFM tips (OTESPA, Bruker Nano Inc., Santa Barbara, CA) with a nominal resonant frequency of 300 kHz, spring constant of 26 N m^{-1}, and nominal tip radius of 7 nm were used. AFM measurements were performed with a scan rate of 1 Hz and in tapping mode.

In each LbL experiment, a fresh quartz crystal was employed. It should be noted that the surface of the LbL films was composed of some rough and smooth regions. As more layers were deposited onto the surface, the proportion of rougher areas increased. A sample photograph taken by the optical microscope of the atomic force microscope is shown in Figure S6 in the Supporting Information. The roughness of these areas could reach as high as a couple of microns for films with eight PE/NP double layers, which was beyond the AFM-measurable range. Thus, we performed AFM analysis on relatively smooth areas only. For each sample, eight different smooth areas were randomly selected for AFM and roughness values were averaged to increase measurement accuracy. We did not try to measure precisely the fraction of "smooth" surface present, but did notice that it decreased with increasing numbers of layers, from perhaps 60% smooth by the end of first double-layer growth step to around 20% smooth after deposition of 8 double layers.

SEM Studies

The surface of LbL films was imaged with a FEI XL30FEG scanning electron microscope, with an accelerating voltage of 10 kV at magnifications of 400 and 80 000. A magnification of 8000 was chosen to obtain SEM cross-section micrographs. Because investigated LbL films were not conductive, prior to performing SEM, their surfaces were coated with a thin layer of gold.

Error Analysis

The standard error for each parameter studied was calculated by using Equation (2). These parameters included the frequency shift of the QCM crystal (Δf), thickness [t; determined by using Eq. (1) and converting the mass per unit area into thickness], and rms roughness values (R) obtained from AFM measurements [Eq. (2)]:

$$\delta(x) = \sqrt{\frac{\sum_{i=1}^{N}(x_i - \bar{x})^2}{N(N-1)}} \quad (2)$$

in which δ is standard error, x is each parameter mentioned above, $\bar{x}$ represents an average value of x, and N is the number of replicate experiments performed to assess the reproducibility of the results. To determine standard error in frequency shift or thickness, two or three replicate tests were performed for a few of the experiments. Due to the time-consuming nature of LbL growth tests, it was practically impossible to repeat all results reported herein, so the error bars given in some of the figures could be taken to be representative. To determine the roughness values, eight different areas of film were tested to ensure accuracy. The standard errors in our LbL growth measurements based on variation of frequency shift were typically below about 15%, as determined by replicate runs. The errors could be attributed mainly to small variations in properties of initial layers that were propagated and amplified in subsequently deposited layers. When salt was added to the solu-

tions, the standard error could reach as high as 30%. Increasing ionic strength was known to reduce the stability of multilayer films[27] and that might have caused the relatively higher error values in these cases.

The standard errors in determining thickness and rms surface roughness of LbL films were generally less than 15 and 10%, respectively. Knowing the errors associated with thickness (t) and rms roughness (R), one can determine the error of the ratio of roughness to thickness by using Equation (3), which is a standard formula for propagation of errors. The calculated error was below 18% for the worst case studied [Eq. (3)]:

$$\delta\left(\frac{R}{t}\right) = \frac{R}{t} \times \sqrt{\left(\frac{\delta(t)}{t}\right)^2 + \left(\frac{\delta(R)}{R}\right)^2} \quad (3)$$

We also performed a number of LbL deposition experiments involving no PEs, but only PS NPs, with opposite charges in alternating layers, the results of which were entirely irreproducible. Insufficient contact area between rigid spherical PS NPs was presumably to blame for low interparticle cohesion that compromised the integrity of the whole film. Whatever NPs managed to be deposited were likely washed off during the rinsing steps. Nonetheless, fairly reproducible growth kinetic data (with errors discussed above) were obtained upon replacing one of the two oppositely charged NP solutions with a like-charged PE solution. PEs seemed to act as a glue between the PS NPs, stabilizing the resultant composites.

Acknowledgements

We would like to thank Prof. Nicholas A. Kotov for providing the quartz crystal microbalance and layer-by-layer assembly robot, and Prof. Steven Schwendeman and Douglas Montjoy for fruitful discussions. We would like to express our gratitude to Dr. Kai Sun and Dr. Haiping Sun from Michigan Center for Materials Characterization for their assistance with AFM and SEM characterization. R.G.L. gratefully acknowledges the support of the National Science Foundation, under grant DMR 1403335. Any opinions, findings, and conclusions or recommendations expressed in this material are those of the authors and do not necessarily reflect the views of the National Science Foundation (NSF). M.M. is a Howard Hughes Medical Institute International Student Research fellow, who is grateful for this support. Moreover, we are grateful for the support provided by Paul R. Lichter, M.D. Research Discovery Fund.

Keywords: kinetics · nanoparticles · polymers · surface analysis · thin films

[1] I. Tokarev, S. Minko, *Soft Matter* **2009**, *5*, 511 – 524.
[2] B. K. Kayaoglu, İ. Gocek, H. Kizil, L. Trabzon, *Tekst. Muhendis* **2012**, *19*, 39 – 47.
[3] M. Rahman, N. Taghavinia, *Eur. Phys. J.* **2009**, *48*, 10602.
[4] M. M. De Villiers, D. P. Otto, S. J. Strydom, Y. M. Lvov, *Adv. Drug Delivery Rev.* **2011**, *63*, 701 – 715.
[5] R. Kniprath, S. Duhm, H. Glowatzki, N. Koch, S. Rogaschewski, J. Rabe, S. Kirstein, *Langmuir* **2007**, *23*, 9860 – 9865.
[6] J. Borges, J. F. Mano, *Chem. Rev.* **2014**, *114*, 8883 – 8942.
[7] J. P. Chapel, J. F. Berret, *Curr. Opin. Colloid Interface Sci.* **2012**, *17*, 97 – 105.
[8] R. R. Costa, J. F. Mano, *Chem. Soc. Rev.* **2014**, *43*, 3453 – 3479.
[9] C. Liang, H. Li, Y. Tao, X. Zhou, Z. Yang, Y. Xiao, F. Li, B. Han, Q. Chen, *J. Mater. Sci.* **2012**, *23*, 1097 – 1107.
[10] K. Na, S. Kim, K. Park, K. Kim, D. G. Woo, I. C. Kwon, H. M. Chung, K. H. Park, *J. Am. Chem. Soc.* **2007**, *129*, 5788 – 5789.
[11] N. Vrana, O. Erdemli, G. Francius, A. Fahs, M. Rabineau, C. Debry, A. Tezcaner, D. Keskin, P. Lavalle, *J. Mater. Chem. B* **2014**, *2*, 999 – 1008.
[12] W. Zhao, J. J. Xu, C. G. Shi, H. Y. Chen, *Langmuir* **2005**, *21*, 9630 – 9634.
[13] J. Ma, P. Cai, W. Qi, D. Kong, H. Wang, *Colloids Surf. A* **2013**, *426*, 6 – 11.
[14] K. R. Knowles, C. C. Hanson, A. L. Fogel, B. Warhol, D. A. Rider, *ACS Appl. Mater. Interfaces* **2012**, *4*, 3575 – 3583.
[15] S. T. Dubas, P. Kumlangdudsana, P. Potiyaraj, *Colloids Surf. A* **2006**, *289*, 105 – 109.
[16] S. T. Dubas, S. Wacharanad, P. Potiyaraj, *Colloids Surf. A* **2011**, *380*, 25 – 28.
[17] P. Nestler, M. Paßvogel, C. A. Helm, *Macromolecules* **2013**, *46*, 5622 – 5629.
[18] L. Shen, P. Chaudouet, J. Ji, C. Picart, *Biomacromolecules* **2011**, *12*, 1322 – 1331.
[19] J. Yu, O. Sanyal, A. P. Izbicki, I. Lee, *Macromol. Rapid Commun.* **2015**, *36*, 1669 – 1674.
[20] X. Zan, D. A. Hoagland, T. Wang, B. Peng, Z. Su, *Polymer* **2012**, *53*, 5109 – 5115.
[21] M. Rahman, F. Tajabadi, L. Shooshtari, N. Taghavinia, *ChemPhysChem* **2011**, *12*, 966 – 973.
[22] A. Salehi, P. S. Desai, J. Li, C. A. Steele, R. G. Larson, *Macromolecules* **2015**, *48*, 400 – 409.
[23] P. Bieker, M. Schönhoff, *Macromolecules* **2010**, *43*, 5052 – 5059.
[24] C. Peng, Y. S. Thio, R. A. Gerhardt, H. Ambaye, V. Lauter, *Chem. Mater.* **2011**, *23*, 4548 – 4556.
[25] S. Ghannoum, Y. Xin, J. Jaber, L. I. Halaoui, *Langmuir* **2003**, *19*, 4804 – 4811.
[26] A. Ostendorf, C. Cramer, G. Decher, M. Schönhoff, *J. Phys. Chem. C* **2015**, *119*, 9543 – 9549.
[27] T. Sennerfors, G. Bogdanovic, F. Tiberg, *Langmuir* **2002**, *18*, 6410 – 6415.
[28] Y. Lvov, K. Ariga, M. Onda, I. Ichinose, T. Kunitake, *Langmuir* **1997**, *13*, 6195 – 6203.
[29] J. Choi, M. F. Rubner, *Macromolecules* **2005**, *38*, 116 – 124.
[30] A. I. Petrov, A. A. Antipov, G. B. Sukhorukov, *Macromolecules* **2003**, *36*, 10079 – 10086.
[31] M. Rubinstein, R. H. Colby, *Polymer Physics*, Oxford University Press, Oxford **2003**.
[32] Q. Wang, *Macromolecules* **2005**, *38*, 8911 – 8922.
[33] C. Picart, J. Mutterer, L. Richert, Y. Luo, G. Prestwich, P. Schaaf, J. C. Voegel, P. Lavalle, *Proc. Natl. Acad. Sci. USA* **2002**, *99*, 12531 – 12535.
[34] M. Rief, F. Oesterhelt, B. Heymann, H. E. Gaub, *Science* **1997**, *275*, 1295 – 1297.
[35] Supplier, private communication, **2016**.
[36] G. Sauerbrey, *Z. Phys.* **1959**, *155*, 206 – 222.
[37] QCM200 Quartz Crystal Microbalance Digital Controller QCM225, 205 MHz Crystal Oscillator, Stanford Research Systems.

Manuscript received: July 19, 2016
Revised: November 3, 2016
Accepted Article published: November 10, 2016
Final Article published: December 13, 2016